Environmental Research 293 (2026) 123787

Contents lists available at ScienceDirect

Environmental Research

journal homepage: www.elsevier.com/locate/envres

Copper- and lead-based nanoparticles in freshwater sediments: Spatiotemporal trends and environmental impact

Mavro Lučić [a,b,*], Janja Vidmar [b,c], Radmila Milačič Ščančar [b,c], Janez Ščančar [b,c], Bor Arah [d], Nevenka Mikac [a], Maja Ivanić [a], Željka Fiket [a], Neda Vdović [a]

[a] Division for Marine and Environmental Research, Ruder Bošković Institute, Bijenička cesta 54, Zagreb, Croatia
[b] Department of Environmental Sciences, Jožef Stefan Institute, Jamova 39, Ljubljana, Slovenia
[c] Jožef Stefan International Postgraduate School, Jamova 39, 1000 Ljubljana, Slovenia
[d] Center for Electron Microscopy and Microanalysis, Jožef Stefan Institute, Jamova 39, Ljubljana, Slovenia

ARTICLE INFO

Keywords:
Metallic nanoparticle
Single-particle ICP-MS
Freshwater sediment
Mixed-effects model
Spatiotemporal distribution
Environmental impact

ABSTRACT

Metallic nanoparticles (MNPs) from anthropogenic activities pose emerging risks to aquatic ecosystems, yet their environmental distribution and occurrence remain poorly characterized due to the analytical complexity of quantifying NPs in sediment matrices. Here, we determine the size and quantify the mass and number concentrations of Cu- and Pb-containing NPs across 31 river and lake sediments in Croatia over a three-year period using single-particle inductively coupled plasma mass spectrometry (sp-ICP-MS). Based on measurements from diverse catchments, Cu NP number concentrations ranged from 1.49×10^8 to 1.06×10^{10} particles/g with particle sizes of 26.8–46.0 nm, while Pb NPs ranged from 1.42×10^8 to 7.63×10^{10} particles/g with smaller sizes of 19.1–26.4 nm. Mixed-effects models revealed spatial heterogeneity dominated temporal patterns, with catchment-scale factors explaining 72–91 % of concentration variance. This spatial structure reflected distinct anthropogenic sources, with Cu NPs from agricultural activities and Pb NPs from legacy mining sites and industrial emissions. In particular, agricultural sites showed elevated levels of bioavailable Cu, with extracted NPs representing up to ~11 % of total Cu, thus identifying hotspots of ecological concern. While Pb NPs are predominantly associated with stable mineral forms such as PbS, the very high concentrations detected at certain sites (up to 25.4 μg g^{-1} for Pb NPs) represent a persistent contamination reservoir with potential for remobilization under changing environmental conditions. This study reports the occurrence of Cu and Pb NPs in freshwater sediments and provides a basis for assessing the environmental risks of MNPs.

1. Introduction

Metal-based nanoparticles (MNPs) have emerged as widespread environmental contaminants in aquatic systems, with freshwater sediments serving as critical repositories that record both contemporary and historical contamination patterns. These particles, typically ranging from 1 to 100 nm, originate from diverse geogenic and anthropogenic sources including industrial processes, mining, urban runoff, vehicle emissions, and agricultural activities (Bundschuh et al., 2018; Li et al., 2023; Worms et al., 2025). Unlike bulk metals, MNPs exhibit unique physicochemical properties that fundamentally alter their environmental behavior, bioavailability, and ecological impact. Particle size directly influences transport mechanisms, aggregation kinetics, and dissolution rates, creating complex exposure scenarios that traditional bulk metal analysis cannot adequately access (Lead et al., 2018; Worms et al., 2025). This complexity has led to significant challenges in accurately assessing environmental concentrations and associated risks. Most environmental NP concentration estimates have been generated indirectly by combining global production data with assumed release rates through modeling approaches that incorporate contaminant transport principles (Gottschalk et al., 2011, 2023; Keller et al., 2023). While these studies provide valuable insights, they are constrained by significant uncertainties arising from oversimplified assumptions and limited consideration of key environmental fate processes, including agglomeration, heteroaggregation, dissolution, and phase transformations (Azimzada et al., 2021). Consequently, reliable risk assessments for NPs require experimental measurements of actual exposure concentrations, supported by spatially and temporally resolved data on particle

* Corresponding author. Division for Marine and Environmental Research, Ruder Bošković Institute, Bijenička cesta 54, Zagreb, Croatia.
E-mail address: mlucic@irb.hr (M. Lučić).

https://doi.org/10.1016/j.envres.2026.123787
Received 14 November 2025; Received in revised form 8 January 2026; Accepted 14 January 2026
Available online 19 January 2026

composition, size distribution, and source identification across different regions (Gottschalk et al., 2011; Li et al., 2023; Lučić et al., 2025).

Research on environmental NPs over the past decade has predominantly focused on specific nanomaterials, with silver (Ag), cerium (Ce), zinc (Zn), and titanium (Ti) NPs dominating the scientific literature (Azimzada et al., 2021; Tou et al., 2021; Vidmar et al., 2022; Zheng et al., 2025). While these studies have established fundamental understanding of key fate processes and distribution patterns of MNPs in aquatic environments, critical knowledge gaps remain regarding copper (Cu) and lead (Pb) NPs in river and lake sediments. Both metals have substantial environmental presence (Lučić et al., 2025; Zhao et al., 2025). This research gap is particularly concerning given the widespread application and environmental relevance of these metals. Cu NPs are increasingly used in antimicrobial coatings, including antifouling paints following the ban of tributyltin, as well as in water treatment systems, agricultural fungicides, and electronic components due to their unique antibacterial, antifungal, and catalytic properties (Ghosh et al., 2025; Keller et al., 2017). Agricultural applications alone represent a major diffuse source to aquatic systems. Their widespread release poses significant ecological risks through multiple pathways. Cu NPs exhibit toxicity to aquatic organisms through multiple pathways, including direct NP effects (oxidative stress, membrane damage, and ion homeostasis disruption) and the release of dissolved Cu^{2+} ions through dissolution, with effects observed across trophic levels from bacteria to fish (Ghosh et al., 2025). Beyond direct toxicity, Cu NPs can disrupt sediment microbial communities and critical biogeochemical processes such as nutrient cycling and organic matter decomposition. Similarly, Pb-containing NPs enter environmental systems through multiple anthropogenic pathways. These include atmospheric deposition from industrial sources, historical use of tetraalkyl lead in gasoline (which represents the largest source of global Pb contamination), weathering of legacy Pb-containing materials, and mining activities (Bačić et al., 2021; Schindler et al., 2022; Zhao et al., 2025; Žerdoner et al., 2025). Pb NPs pose particularly severe toxicological risks due to their neurotoxic effects on aquatic organisms, particularly during critical early life stages (Ng et al., 2018). Additionally, Pb NPs have been shown to inhibit acetylcholinesterase activity and induce oxidative stress in aquatic organisms, with effects linked to swimming dysfunction and broader physiological impairments (Chiang et al., 2016). Despite the rapid increase in global production and environmental release of Cu-based and Pb-based NPs and their well-documented ecotoxicological concerns, systematic field studies reporting measured concentrations, size distributions, and spatiotemporal trends in freshwater sediments are still lacking. These data are essential for accurate risk assessment of these ubiquitous contaminants.

The development of single particle inductively coupled plasma mass spectrometry (sp-ICP-MS) has revolutionized the ability to characterize MNPs in complex environmental matrices. This technique provides simultaneous quantification of particle size distributions, number concentrations, and mass concentration, enabling discrimination between particulate and dissolved metal fractions that is crucial for understanding environmental fate processes (Li et al., 2025). Size analysis of MNPs using sp-ICP-MS relies on the fundamental assumption that all detected nanoparticles are spherical with known chemical compositions. This assumption becomes problematic when analyzing environmental samples, where MNPs exhibit complex and variable compositions that deviate from idealized conditions (Worms et al., 2025). Additional limitations include sp-ICP-MS monitoring only single metal isotopes per acquisition, providing no compositional information on element associations within individual particles. Analysis requires non-acidified sample introduction to preserve particle integrity, which can result in particle losses through aggregation, settling, and adsorption in the introduction system. Despite these size characterization and compositional limitations, sp-ICP-MS remains a powerful and reliable technique for quantitative analysis of MNP concentrations in environmental samples.

To address these identified knowledge gaps, this study employed sp-ICP-MS analysis to quantify Cu and Pb NP concentrations, size distributions, and spatiotemporal patterns in freshwater sediments across multiple river and lake systems in Croatia over a three-year sampling period (2019–2021). This was complemented by scanning electron microscopy coupled with energy dispersive X-ray spectroscopy (SEM-EDS) for source identification and particle characterization. To our knowledge, this represents the first investigation of Cu and Pb NP occurrence in real-world freshwater sediments spanning diverse geochemical compositions, providing critical baseline data on the extent and variability of these contaminants in aquatic environments. At the regional scale, this work addresses critical data requirements for transboundary river basin management such as the large catchments (e.g. Danube, Drava, Sava, Neretva), where coordinated monitoring frameworks require standardized methodologies and baseline concentrations for emerging contaminants across multiple countries.

The specific objectives were to: (1) characterize and quantify Cu and Pb NPs in freshwater sediment samples across multiple river and lake systems, (2) assess temporal trends in MNP contamination, (3) evaluate spatial distribution patterns and controlling factors, and (4) assess potential environmental risks and fate implications for Cu and Pb NPs in freshwater systems.

2. Materials and methods

2.1. Sample collection

The sampling strategy covered diverse geological and environmental settings, including degree of anthropogenic influence (Fig. A1, Table A1). This aimed to establish thresholds that distinguish natural levels of MNPs from anthropogenic contamination. The sediment samples were collected from 31 locations across diverse lithological units and geochemically variable regions, comprising 26 river sediments, 3 lake sediments, and 2 artificial reservoir sediments (Fig. 1, Table A1). Multiple sampling points were established along larger rivers to ensure comprehensive coverage. Major river systems include the Sava River, which flows through Zagreb (~1.1 million inhabitants) and Slavonski Brod (~49,000 inhabitants) and receives urban-industrial effluents; the Drava River, which carries legacy contamination from historical Pb-Zn mining operations in Slovenia; and the Danube River, which is impacted by agricultural runoff, municipal wastewater, and industrial discharges. Additional urban-industrial centers include Karlovac (~49,000 inhabitants), characterized by historical textile, chemical, and metal-processing industries; Sisak (~47,000 inhabitants), with historical iron and steel production; and Osijek (~108,000 inhabitants), dominated by agriculture and chemical manufacturing. The sampling design encompasses geochemically diverse units, spanning carbonate-dominated Dinaric karst regions to siliciclastic Pannonian Basin sediments (Fig. A1). Sediment samples were collected during summer low-flow conditions (July–August) in 2019, 2020, and 2021 to minimize seasonal hydrological variability and ensure comparability across sampling years. River sediments were collected using a spatula along the river channel in areas protected from strong currents where fine-grained material naturally accumulates. At each location, a minimum of three subsamples were collected at 50 m intervals, according to standard practice in sediment sampling and homogenized to produce a composite sample representative of the sampling site (ISO 5667-12, 2017). Lake sediments were obtained from boats using a Van Veen grab sampler, with sampling focused on the approximate central lake areas. Immediately following collection, sediments were wet-sieved using ambient water to prevent chemical alteration, and suspensions containing particles <63 μm were preserved in 1 L plastic bottles. In the laboratory, suspensions were allowed to settle under gravity, excess water was carefully decanted, and the remaining material was freeze-dried (Freezone 2.5, Labconco Corporation, Kansas City, MO, USA) and stored at 4 °C in the dark until analysis to minimize oxidation and degradation.

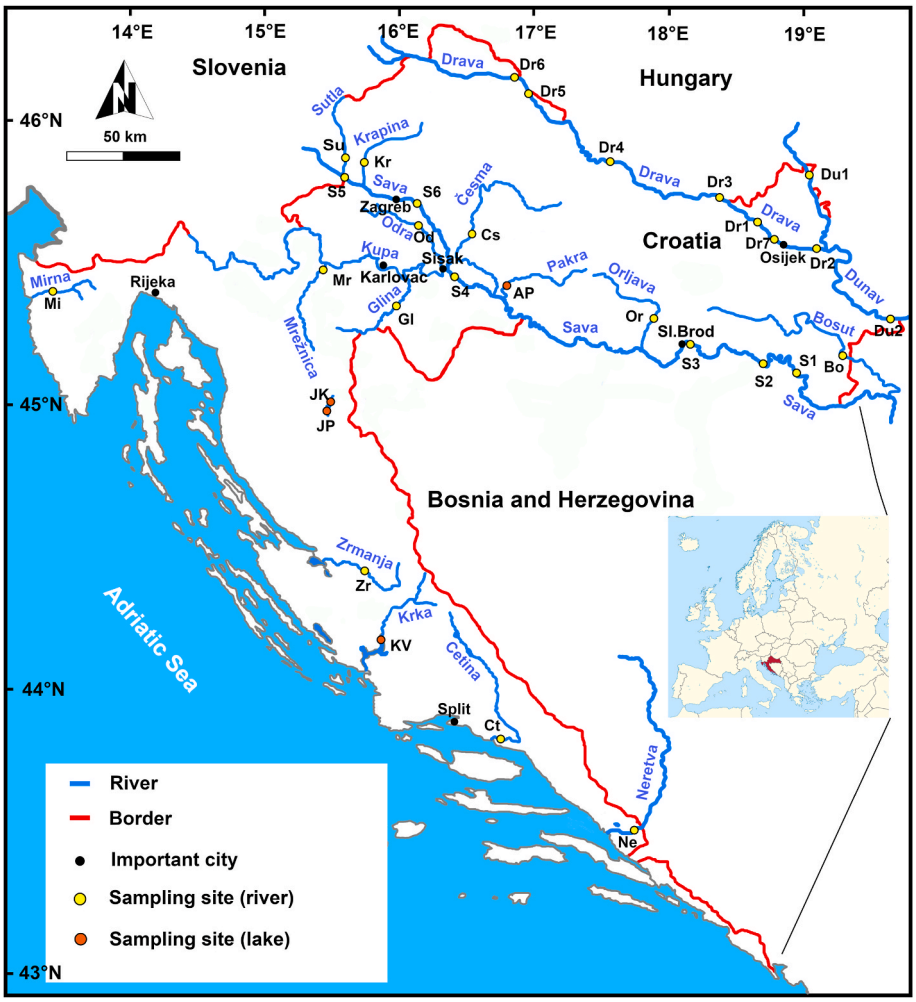

Fig. 1. Sediment sampling locations.

2.2. Metal analysis of bulk samples

Metal concentrations of Pb and Cu in bulk samples were determined using high-resolution inductively coupled plasma mass spectrometry (HR-ICP-MS) with an Element 2 instrument (Thermo Finnigan, Bremen, Germany). Prior to analysis, samples were digested using a microwave digestion system (Multiwave 3000, Anton Paar, Graz, Austria) following a two-step procedure with identical heating programs (15-min ramp to 180 °C, 40-min hold): (I) 5 mL HNO_3 (65 %, pro analysis, Kemika, Zagreb, Croatia) + 1 mL HCl (37 %, VLSI Grade, Rotipuran, Carl Roth, Karlsruhe, Germany) + 1 mL HF (47–51 %, for trace analysis, Fluka, Buchs, Switzerland); (II) 6 mL H_3BO_3 (40 g L^{-1}, Fluka). Following digestion, samples were diluted ten-fold, acidified with HNO_3 (67 %, s. p., Fluka), to obtain 2 % (v/v) HNO_3, and indium (In, 1 μg L^{-1}) was added as an internal standard. Analytical quality control was ensured through simultaneous analysis of procedural blanks and certified reference materials, including soil reference material NCS DC 773902 (GBW 7410) and stream sediment reference material NCS DC 73309 (GBW 07311). Recovery rates ranged from 90 to 100 % depending on the target element. Detailed methodological information is provided elsewhere (Fiket et al., 2017).

2.3. Extraction of Cu and Pb NPs from sediment samples

The extraction procedure for NPs was based on a previously developed protocol for solid environmental samples (Lučić et al., 2025). Each sample was extracted and analyzed in duplicate. Extraction efficiency of NPs from sediments with varying geochemical compositions was evaluated using Cu and Pb NP suspensions spiked to sediments and analyzed in triplicate. Two sediment types were tested: carbonate-rich (KV) and siliciclastic sediment (GI) (Fig. 1; Table A1), which characteristics are described in detail in Vdović et al. (2021). Suspensions of CuO NPs (20 wt%, US Research Nanomaterials, Houston, TX, USA; nominal size 25–55 nm determined by transmission electron microscopy (TEM)) and PbO NPs (2 wt%, Nanoshel – Intelligent Materials Private Limited, Punjab, India; nominal size 45–55 nm determined by scanning electron microscopy (SEM)) were added to sediment to achieve a target concentration of 100 μg g^{-1} for both Cu and Pb NPs. After 24 h of NP incubation, sediment samples (200 mg) were dispersed in 20 mL of 2.5 mM tetrasodium pyrophosphate (TSPP) and agitated for 24 h at 300 rpm using an orbital shaker (Edmund Bühler GmbH, Germany), followed by sonication for 20 min in an ultrasonic water bath (Iskra PIO, Šentjernej, Slovenia). After settling for 3 h according to Stokes' law, the supernatant was collected from a height of 0.5 cm above the settled material, corresponding to particles <450 nm. Details can be found in Lučić et al. (2025).

2.4. Electron microscopy analysis

Based on elevated metal concentrations, samples from sites Mi, Ne, D6, Kr, Su, and Cs were selected for detailed scanning electron microscopy (SEM, Apreo 2S) coupled with energy dispersive X-ray spectroscopy (EDXS, Ultim Max SDD 100 mm^2). The supernatants obtained from the sediment extracts were shaken with Milli-Q water for 24 h. One to

two drops of each supernatant were then deposited onto silicon wafers and analyzed for morphological structure and chemical composition.

2.5. Sp-ICP-MS analysis

Single particle ICP-MS measurements were performed using a model 7900 ICP-MS instrument from Agilent Technologies (Santa Clara, CA, USA) equipped with a quadrupole mass analyzer. Operating parameters (summarized in Table A2) were optimized for plasma robustness and sufficient sensitivity. Cu and Pb in aqueous standard solutions were analyzed for their most abundant isotopes: ^{63}Cu (69.2 %) and ^{208}Pb (52.4 %). Cu was analyzed in helium collision mode (4.3 mL min^{-1} He gas flow), while Pb was analyzed in no-gas mode. Because environmental particles consist of various chemical forms (oxides, sulfides, mixed phases), all sp-ICP-MS measurements report Cu and Pb NP concentrations and calculate particle sizes by assuming pure metallic composition (Cu: 8.96 g cm^{-3}; Pb: 11.34 g cm^{-3}) for standardization. The detection limits for particle size were 19.9 nm for Cu and 12.3 nm for Pb. Measurements were conducted in time-resolved analysis (TRA) mode to collect intensity signals from individual particles as they were vaporized and ionized in the plasma. A short integration dwell time of 100 μs per reading was employed. Sample flow rate was determined daily by pumping a known mass of Milli-Q water at room temperature (N = 3) at a peristaltic pump speed of 0.1 rotations/s. Transport efficiency was determined using the "particle size' method (Pace et al., 2011) with a suspension of 53 nm gold nanoparticles (Au NPs) supplied by nanoComposix (San Diego, CA, USA) at a known concentration (0.05 mg mL^{-1}). The suspension was appropriately diluted with milli-Q water to achieve an Au NP concentration of 132 ng L^{-1}. For calibration, dissolved Au standards (0, 0.1, 0.5, 1, 5, and 10 μg L^{-1}) were prepared from a stock standard solution of ionic Au (1000 mg L^{-1}) in 2 % (v/v) HCl/0.5 % (w/v) thiourea solution (Inorganic Ventures, Christiansburg, VA, USA) using Milli-Q water. For all samples, dilution factors (5000 × for Cu and 10000 × for Pb) were adjusted to ensure that the number of detected particles during 1–2 min of acquisition exceeded 100 (to reduce random error governed by Poisson statistics to ≤10 %) while remaining below 3800 (to limit relative bias from multiple particle events to <3 %), assuming a transport efficiency of 0.10 (10 %), sample flow rate of 0.33 mL min^{-1}, and dwell time of 100 μs (Table A2).

Signal intensity data from sp-ICP-MS measurements were processed using spCal software (Lockwood et al., 2021), an open-source Python--based platform that provides transparent data processing through its interactive graphical interface. Particle events were identified and separated from background signals using Poisson-based statistical filtering. The detection thresholds were 6 counts for Cu NPs and 7 counts for Pb NPs. Particle diameters were subsequently calculated from the particle mass assuming spherical geometry, incorporating element-specific mass fractions and density values. Nanoparticle recovery was evaluated using multiple metrics for comprehensive characterization. The mean particle diameter recovery (R_D) was calculated as follows:

$$R_D\ (\%) = \frac{R_{Sed}}{R_S}\ \text{x100} \quad (1)$$

where R_{sed} is the mean diameter of particles detected in the spiked sediment sample, and R_S is the mean diameter of particles in the spike solution prepared in Milli-Q water. The particle number concentration recovery and two mass recovery metrics (particle mass and total mass recoveries) were calculated using the following equation:

$$R_M\ (\%) = \frac{(R_{Sed} - R_C)}{R_S}\ \text{x100} \quad (2)$$

where R_{sed} is the concentration of the relevant metric (number of particles, particle mass, or total mass of element) in the spiked sediment sample, R_C is the concentration of the same metric in the non-spiked control sediment sample, and R_S is the concentration of the same metric in the spike solution. Total mass recovery is based on the mean signal value from the time-resolved analysis data over the specified range and represents the sum of particulate and ionic mass recovered.

To estimate the relative proportion of potentially bioavailable metal fractions, we compared the mass of detected NPs with the total metal mass determined by sp-ICP-MS according to the equation:

$$\text{Dissolved fraction} = 1 - (\text{NP mass} / \text{Total metal mass}) \quad (3)$$

The dissolved fraction, defined as the difference between these values, represents metal present as dissolved ions and NPs below the instrument's size detection limit. Details are provided in Appendix A.

2.6. Statistical analysis

All particle number, mass concentration, and size data were log-transformed to meet statistical assumptions. Analyses were performed in R (R Core Team, 2023), with results considered statistically significant at $p < 0.05$. Model assumptions were verified using residual plots. Linear mixed-effects models were used to analyze temporal changes of Cu and Pb NPs (Brown, 2021). Because multiple samples were collected from the same river/lake across different years, these models accounted for within-site correlation. Three model structures were compared using Akaike Information Criterion (AIC): (1) simple linear regression, (2) mixed-effects models with random river/lake intercepts, and (3) linear models with fixed river/lake effects. The best-fitting model was selected for each response variable, and temporal trends were calculated as annual percent change with 95 % confidence intervals. To determine whether overall trends were consistent across individual catchments, separate linear regressions were fitted for each river/lake. Spatial variation in MNP distributions was assessed using the same mixed-effects modeling framework. River/lake effects were evaluated using likelihood ratio tests for random effects models or ANOVA F-tests for fixed effects models. The proportion of variance explained by spatial differences was quantified through variance decomposition and pairwise differences between river/lakes were evaluated using Tukey's post-hoc tests when appropriate.

Cumulative probability plots of particle mass concentrations were used to identify geochemical anomalies by detecting gaps or breaks in the distribution, where anomalous values separate from the main concentration mode. Unlike parametric methods that identify outliers even in normal distributions, this approach detects only discontinuities indicative of genuinely distinct populations, thus avoiding false positives in unimodal data (Matys Grygar et al., 2023).

3. Results and discussion

3.1. Cu and Pb NPs recovery from spiked sediments

To evaluate the extraction efficiency of NPs from sediments with varying geochemical compositions, spike recovery experiments were conducted using Cu and Pb-based NPs (Table A3). Before spiking, both NP suspensions were characterized by sp-ICP-MS to verify their particle size distributions. The measured mean size was 53.3 ± 30.9 nm for CuO NPs, consistent with the nominal 25–55 nm range determined by TEM, and 27.5 ± 12.0 nm for PbO NPs, which is slightly smaller than the nominal 45–55 nm range determined by SEM, possibly reflecting differences in measurement methods. Time-resolved scans and size distributions are provided in Fig. A2–A7. Spike recovery experiments using freshly added NPs may not fully represent extraction efficiency for aged environmental NPs that have undergone prolonged weathering and strong matrix binding; nevertheless, they provide valuable insights into how sediment geochemistry influences extraction performance and NP characteristics. Two distinct sediment types were tested: carbonate-rich sediment from Visovac Lake (KV; 331 g kg^{-1} of Ca) and siliciclastic

sediment from Glina River (Gl; 11.4 g kg^{-1} of Ca). Particle size recoveries varied from 91.3 to 101.3 % for Cu NPs and 105.1–111.7 % for Pb NPs across both sediment matrices. Particle number recoveries ranged from 103.4 to 107.8 % for Cu NPs and 61.4–63.7 % for Pb NPs, while particle mass recoveries were 100.6–132.6 % for Cu NPs and 70.6–105.5 % for Pb NPs. These recovery rates demonstrate consistent extraction efficiency across different sediment geochemistries. Although extraction methodologies have been reported for Cu NPs in soils (Navratilova et al., 2015) and marine sediments (Li et al., 2023), and for Pb NPs in sewage sludge (Lučić et al., 2025), validation across solid environmental matrices with contrasting geochemical compositions remains limited. Recovery data for Pb NPs in freshwater sediments are entirely absent from the literature. The present recovery rates, ranging from 91 to 132 % across both carbonate-rich and siliciclastic matrices, indicate the robustness of the extraction methodology for diverse freshwater sediment types and provide a foundation for future environmental investigation of MNPs.

3.2. Concentration of Cu- and Pb NPs and SEM-EDS characterization

3.2.1. Concentrations of Cu and Pb in bulk sediment and NP fraction

Complete ICP-MS and sp-ICP-MS data for Cu- and Pb-containing NPs across all samples and three sampling years are provided in Appendix A. Total Cu concentrations ranged from 4.4 to 79.9 μg g^{-1} (mean: 30.3 μg g^{-1}), comparable to Croatian soil averages (29.7 μg g^{-1}), with elevated levels reflecting anthropogenic inputs from agriculture and industry (Halamić et al., 2012). Pb concentrations showed greater variability (10.7–359 μg g^{-1}; mean: 60.1 μg g^{-1}), exceeding the Croatian average (38.4 μg g^{-1}) due to legacy mining and industrial emissions. All sites remained below the Probable Effect Concentration (PEC) for Cu (149 μg g^{-1}), while two locations (Dr6 and Kr) exceeded the Pb PEC threshold (128 μg g^{-1}), indicating probable adverse biological effects (MacDonald et al., 2000).

NP concentrations followed similar spatial patterns to total metals but at proportionally lower levels. Cu NPs ranged from 0.091 μg g^{-1} at JK to 4.63 μg g^{-1} at KR, while Pb NPs varied from 0.078 μg g^{-1} at JP to 25.4 μg g^{-1} at D6. Cu NPs exhibited sizes ranging from 26.8 to 46.0 nm (mean 33.1 nm), while Pb NPs were consistently smaller, ranging from 19.1 to 26.4 nm (mean 22.5 nm). Cumulative probability analysis identified inflection points corresponding to Tukey inner fence (TIF) boundaries at 1.94 μg g^{-1} for Cu NPs and 6.46 μg g^{-1} for Pb NPs (Fig. 2). These thresholds were exceeded at six locations for Cu NPs (S, Kr, Su, Dr, Du, Mi) and three locations for Pb NPs (Kr, Dr5, Dr6) (Fig. A8). For comparison, the 95th and 98th percentiles occurred at higher concentrations (Cu: 2.11 and 2.51 μg g^{-1}; Pb: 8.53 and 12.64 μg g^{-1}). These TIF-derived thresholds, based on distribution breaks rather than arbitrary percentiles, provide robust criteria for identifying anthropogenically enriched sites that require targeted risk assessment. Derived from sites spanning diverse geochemical compositions, these thresholds may be applicable to other freshwater systems. The highest NPs concentrations generally corresponded to locations with elevated total metal levels, indicating that NPs abundance is closely linked to overall contamination intensity.

This study revealed substantially higher NP mass concentrations than those previously reported for sediments. Study of marine sediments (Li et al., 2023) showed the particle number concentrations ranging from 2.91 × 10^6 to 1.81 × 10^8 particles/g and mass concentrations of 0.001–0.102 μg g^{-1}, with larger particle sizes of 46.8–85.1 nm. Similarly, a study on Daya Bay sediments in China (Ying et al., 2024) reported Pb NP concentrations ranging from 4.70 × 10^7 to 1.66 × 10^8 particles/g with particle sizes of 47–78 nm, and Cu NPs ranging from 2.72 × 10^7 to 3.76 × 10^8 particles/g with sizes of 33–42 nm. The NP size distributions in our study align well with the Daya Bay findings for Cu NPs but show notably smaller size ranges than those observed in Laizhou Bay (Li et al., 2023) and much smaller ranges for Pb NPs compared to Daya Bay (Ying et al., 2024). These differences likely reflect variations in contamination sources and environmental conditions influencing particle size distributions. The contrasting geochemical conditions between freshwater and marine environments play a critical role. The high ionic strength in seawater promotes particle aggregation and sedimentation, while dissolved organic matter in both systems can stabilize NPs through electrostatic repulsion, thereby affecting their size distributions and transport behavior (Amiri and Behin, 2025; Li et al., 2023). The smaller NP sizes observed in freshwater sediments may pose greater ecological risks due to enhanced bioavailability, increased organism-particle interactions, and size-dependent toxicity mechanisms (Bundschuh et al., 2016).

3.2.2. SEM-EDS characterization of contaminated samples

Based on elevated bulk metal and NP mass concentrations, samples from six sites (Mi, Ne, D6, Kr, Su, and Cs) were subjected to detailed SEM-EDS analysis to determine particle compositions and potential anthropogenic sources (Fig. A9–A12 and Table A4–A7). We focused on characterizing sites with visible anthropogenic contamination signals to

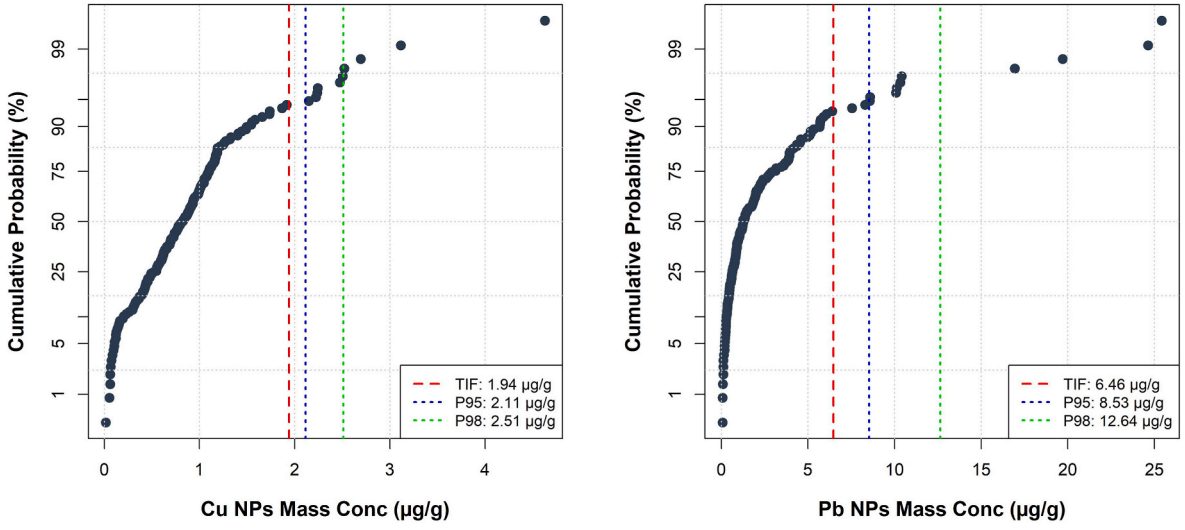

Fig. 2. Cumulative probability distributions of Cu and Pb NP mass concentrations in analyzed sediments. Vertical dashed lines represent Tukey Inner Fence (TIF), 95th percentile (P95), and 98th percentile (P98) values. The TIF values (1.94 μg g^{-1} for Cu NPs and 6.46 μg g^{-1} for Pb NPs) identify statistically significant shifts in the distribution, marking the transition from background to elevated contamination levels. P95 and P98 represent more rigorous thresholds.

identify source-specific particle signatures, rather than analyzing naturally occurring Cu- and Pb-containing particles that may be present at background levels. Although natural weathering of Cu- and Pb-bearing minerals contributes to the total NP pool, the selected sites are locations where anthropogenic inputs likely influence their elevated concentrations, and most exceed statistically determined threshold values. The elemental composition of Cu-bearing particles suggested possible agricultural origins. Notably, sediments at the Cs location (Fig. A9) contained Cu-Zn particles with high metal concentrations (Cu: 13.71 at %; Zn: 8.17 at%, Table A4), a signature consistent with Cu-Zn fungicide formulations widely used in vineyard disease control (Imfeld et al., 2020). Particles at site Ne (Fig. A10) had slightly lower concentrations of Cu-bearing particles (3.41–6.70 at%, Table A5) that were systematically associated with elevated Ca content (14.0–23.7 at%), suggesting agricultural runoff where Cu-rich particles likely become mixed with limestone amendments and the carbonate-rich soils (Imfeld et al., 2020).

Pb-containing particles from the D6 (Fig. A11, Table A6) exhibited characteristic Pb:S ratios of 1.12 (atomic), which closely match galena (PbS) stoichiometry and confirm their origin from weathered Pb-Zn mining operations in the upstream Meža River in Slovenia (Bao et al., 2021; Žerdoner et al., 2025). In contrast, Kr sediments (Fig. A12, Table A7) contained Pb-Sb intermetallic particles with atomic contents of 1.75 at% Pb and 1.65 at% Sb (1.06 ratio), suggesting use of bulk Pb–Sb alloys in applications such as cable sheaths, lead-acid battery grids, and automotive accumulators (Chen et al., 2025).

3.3. Spatiotemporal variations in Cu- and Pb-containing NPs

3.3.1. Temporal variations of MNPs

Metallic NP concentrations in river sediments displayed contrasting temporal patterns over 2019–2021 (Fig. 3 and A13), with Cu and Pb NPs showing different environmental behaviors. Cu NPs showed complex temporal dynamics characterized by non-significant overall trends: mass concentrations exhibited a slight increasing tendency (2.65 % annually, $p = 0.521$) while particle concentrations showed a declining trend (−4.18 % annually, $p = 0.120$) (Table A8). Analysis of individual rivers and lakes revealed significant temporal trends in a limited number of catchments: 3 out of 19 (16 %) for mass concentrations and 4 out of 19 (21 %) for number concentrations, exhibiting mixed patterns of both increases and decreases (Table A9). However, Cu NP particle sizes showed significant overall increases of 2.18 % annually ($p < 0.001$), with mean sizes increasing from 30–34 nm in 2019 to 34–46 nm by 2021 in multiple locations, particularly evident in JP and Bo (Fig. 4). In aquatic environments, CuO NPs undergo aggregation processes strongly influenced by water chemistry parameters including pH, natural organic matter and phosphate concentrations (Conway et al., 2015; Wang et al., 2016). Similar temporal increases in NP size have been observed in modeling studies of freshwater lake systems, where nanoCuO from antifouling paints accumulated predominantly in sediments due to particle attachment through sorption and heteroaggregation, with concentrations continuously increasing over a 101-year period (Ross and Knightes, 2022). These aggregation processes are particularly relevant for this study, where lower hydrodynamic energy promotes particle interactions that increase mean NP sizes.

In contrast, Pb NPs demonstrated significant overall declining trends across both concentration metrics: mass concentrations declined by 7.86 % annually ($p = 0.024$) and particle concentrations decreased by 7.66 % annually ($p = 0.003$), suggesting regional reduction in contamination (Table A10). Despite these significant overall trends in mass and number concentrations, individual river/lake analysis revealed that only 3 and 4 out of 19 catchments (16 and 21 %) showed statistically significant trends for these metrics, with mixed patterns of both increases and decreases. Notable declines in mass and number concentrations occurred at sites Bo, Cs and JK (−24.3 % to −48.8 %). Pb NP sizes remained temporally stable (0.09 % annual change, $p = 0.789$), with only two lakes (AP and JP) showing significant size trends with low percent change (Table A10). This demonstrates that Pb NPs maintain consistent physicochemical properties during transport and deposition.

These contrasting temporal patterns reflect fundamentally different fate processes. Cu NPs are prone to aggregation with increasing particle sizes despite relatively stable mass concentrations, whereas Pb NPs show declining concentrations with stable particle characteristics. Global temporal analysis of heavy metals in river sediments from 1970 to 2018 demonstrates that primary pollution sources have shifted from mining and manufacturing to waste discharge, with rigorous emission standards proving effective at controlling point sources of contamination (Niu et al., 2021). The declining Pb NP trends observed in our study validate this pattern and likely reflect sustained reductions in atmospheric deposition resulting from the global phase-out of leaded gasoline, which historically accounted for most Pb pollution entering aquatic systems through atmospheric transport and subsequent deposition (Bačić et al., 2021; Schindler et al., 2022). However, exceptionally low discharge rates in some freshwater environments during 2021 cannot be excluded as a contributing factor, as reduced flow typically results in lower contaminant mobility (Lučić et al., 2022; Trostle et al., 2018). In contrast, Cu NPs represent ongoing environmental challenges from diffuse agricultural sources (including fungicides, pesticides, and biosolids) and industrial applications (particularly antifouling paints) that remain less comprehensively regulated. While annual sampling effectively captures broad temporal trends, it misses seasonal variations and episodic hydrological events that can significantly influence NP transport and deposition. More frequent sampling would help distinguish source reductions from transport-related concentration changes, providing better insight into short-term NP dynamics.

3.3.2. Spatial variations of MNPs

River sediments showed strong spatial variability in MNP distributions across the study region, with Cu and Pb NPs displaying distinct patterns across catchments (Fig. 5 and A14). Cu NPs demonstrated evidence for spatial variation, with fixed river/lake effects providing optimal model fit (all river/lake effects $p < 0.001$) (Table A11). Spatial variance analysis demonstrated that river/lake explained 72 % of total variance in mass concentrations, 85 % in particle number concentrations, and 44 % in particle size variation (Fig. 6; Table A12). Individual river/lake analysis revealed 42–50 % of catchment pairs differed significantly after Tukey adjustment, indicating moderate heterogeneity in pairwise comparisons. Notable spatial patterns included Kr as the most contaminated Cu NP location (4–10 × 10^9 particles/g, 1.06–4.63 μg g^{-1}), followed by major rivers Sava (2–6 × 10^9 particles/g, 0.43–2.67 μg g^{-1}) and Drava (3–8 × 10^9 particles/g, 0.62–2.47 μg g^{-1}), while protected areas like JP and JK maintained consistently low concentrations (0.1–0.8 × 10^9 particles/g, 0.02–0.39 μg g^{-1}). The approximately 10–50-fold concentration differences observed between highly impacted (Kr) and pristine sites (JP, JK) fall within the range of spatial variability predicted by probabilistic material flow models for Swiss rivers, where NP concentrations varied by factors of up to 370 across 543 river sections due to spatially variable emissions and local dilution (Gottschalk et al., 2011). The high proportion of variance explained by Cu NP concentrations reflects their fundamental controls: (1) geographic distribution of emission sources, such as agricultural activities (copper-based fungicides and pesticides), industrial effluents, urban wastewater discharge, and nanoCu-based antifouling paints, which vary with population density, land and water use patterns; and (2) local dilution capacity, which differs based on catchment characteristics and hydrological regime (Gottschalk et al., 2011; Lučić et al., 2022; Trostle et al., 2018).

Pb NPs demonstrated even more extreme spatial dominance with fixed river/lake effects explaining 89 % of mass concentration, 91 % of particle number concentration, and 80 % of particle size variance (Table A12). Individual river/lake analysis showed that 60–66 % of catchment pairs are statistically different, indicating more extensive spatial heterogeneity than Cu NPs. The most heavily contaminated sites

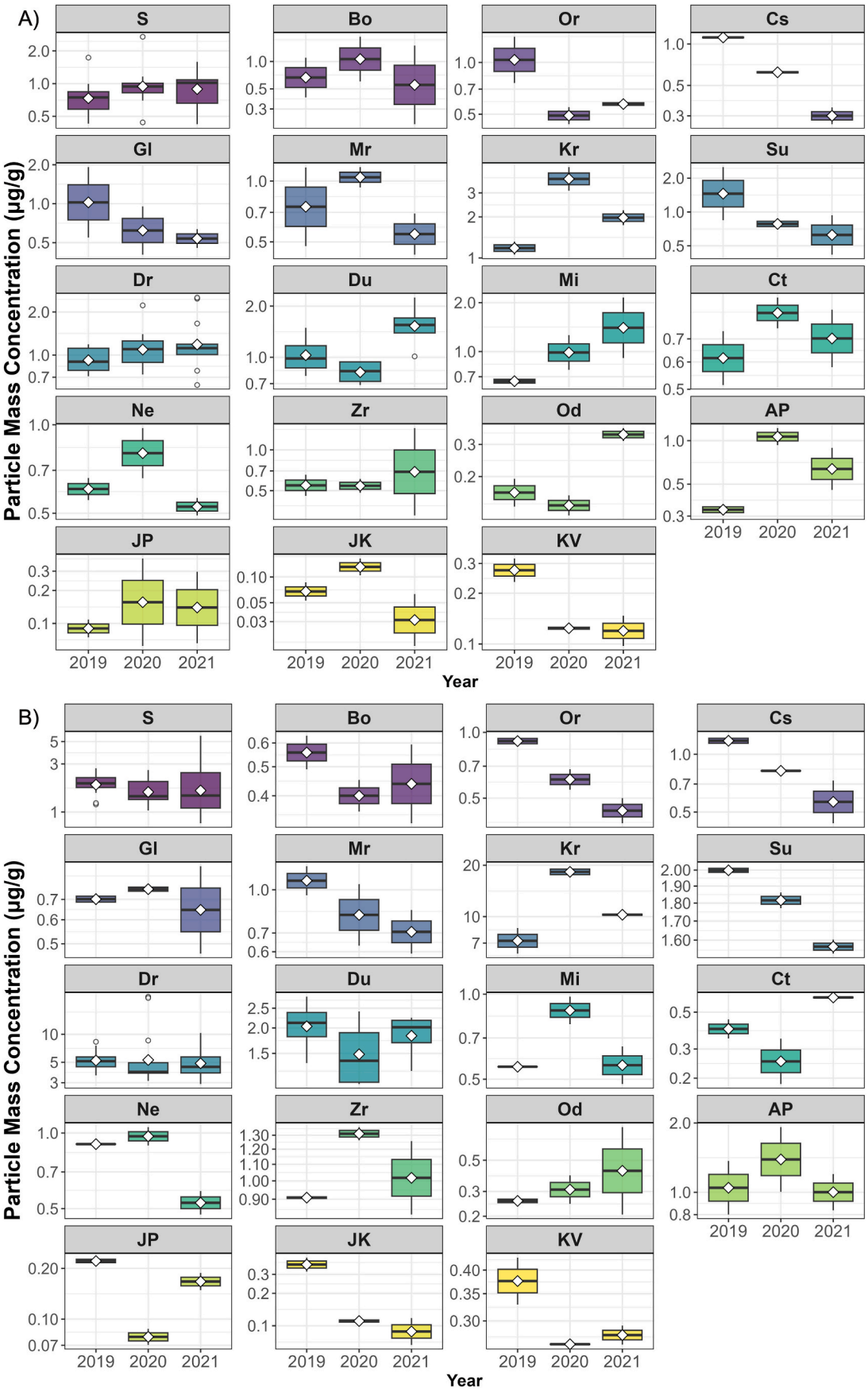

Fig. 3. Temporal trends of (A) Cu and (B) Pb NP mass concentrations across three sampling years.

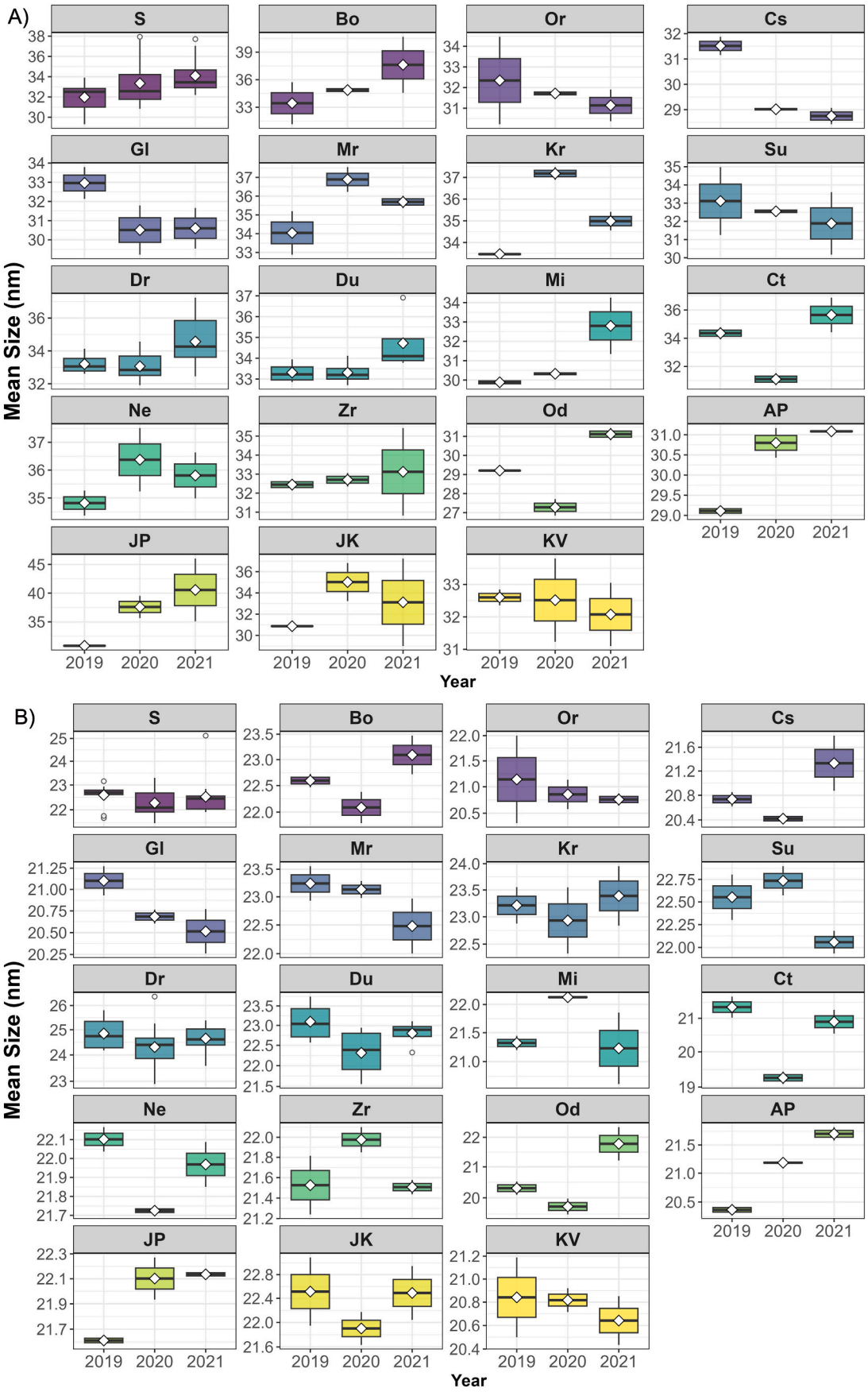

Fig. 4. Temporal trends of (A) Cu and (B) Pb NP size distribution across three sampling years.

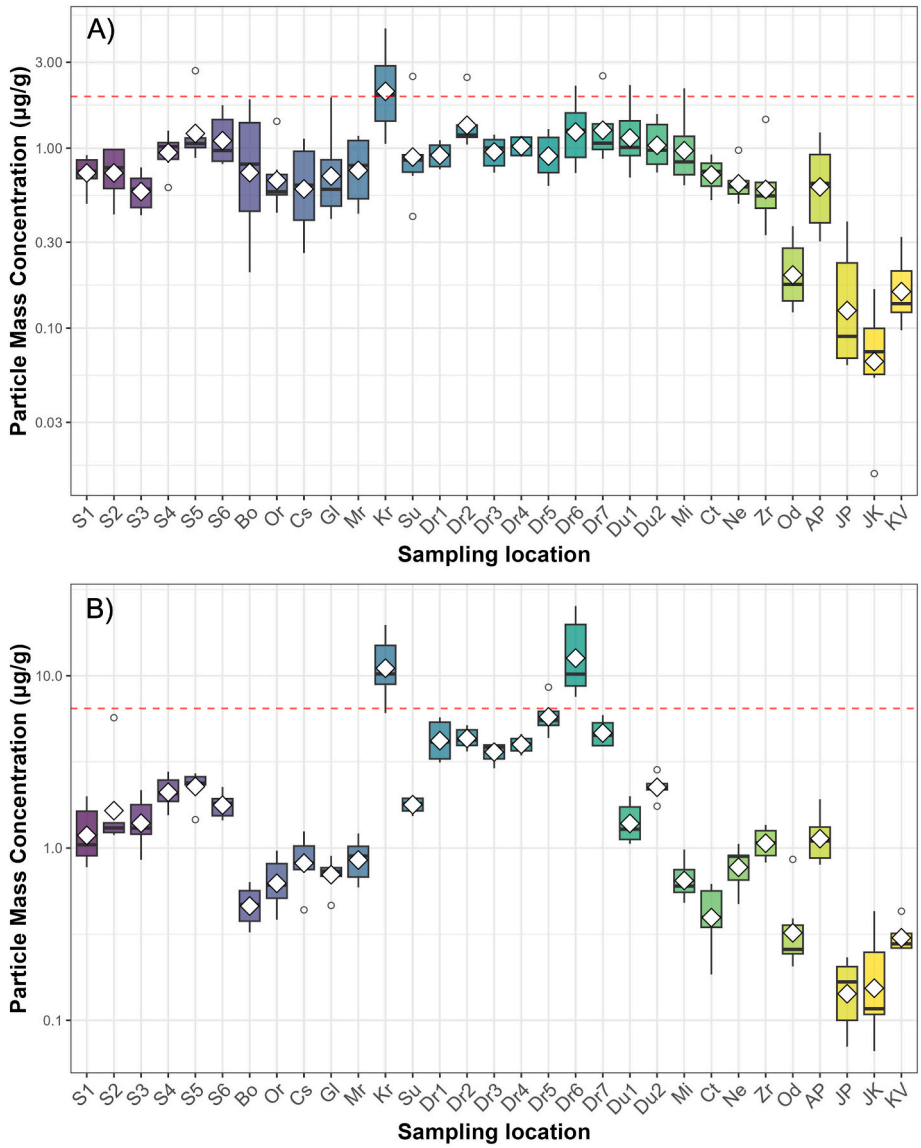

Fig. 5. Spatial trends of (A) Cu and (B) Pb NP mass concentrations across different catchment areas. Red dashed line separates the geochemical background (1.94 µg g^{-1} for Cu; 6.46 µg g^{-1} for Pb) from certain locations that are possibly contaminated.

Dr6 and Kr contained 6.83–7.63 × 10^{10} particles/g with 19.7–25.4 µg g^{-1} mass concentrations (Fig. 5 and A14). This extreme contamination at Dr6 is supported by upstream PM_{10} measurements along the Meža River, located approximately 150 km upstream (Žerdoner et al., 2025), where airborne Pb NPs showed elevated concentrations (26.3–131 µg g^{-1}), establishing a clear source-to-sink relationship. Major rivers including the Sava and Drava exhibited intermediate to high Pb NP loads (2–5 × 10^{10} particles/g), around 300 times higher than pristine sites, which had concentrations of 1–3 × 10^{9} particles/g and mass concentrations of 0.03–0.43 µg g^{-1}. Notably, even Pb NP particle sizes showed strong spatial structure (80 % variance explained) with 38 % of catchment pairs significantly different, demonstrating that sources and processes governing their distributions are highly site-specific. This spatial heterogeneity reflects the fundamental role of local factors in governing NP distributional patterns, including industrial point sources (particularly lead smelters and battery manufacturing), historical mining legacies, atmospheric deposition, land use patterns, and geological characteristics (Bundschuh et al., 2018; Lučić et al., 2022; Žerdoner et al., 2025). Additionally, the combination of different aging processes compared to Cu NPs, greater stability of Pb NPs in aquatic environments, and more direct source-to-sediment pathways (e.g., atmospheric deposition) limits the homogenization processes that would otherwise equilibrate size distributions across catchments. The consistently stronger spatial structure for Pb NPs suggests minimal downstream transformation, whereas Cu NP distributions reflect more diffuse sources (agriculture, urban runoff) that are effectively homogenized through hydrological processes.

3.4. Environmental impact of Cu and Pb NPs

To assess the environmental impact of Cu and Pb NPs in the analyzed sediments, we quantified the proportion of NPs relative to the total metal content (determined after acid digestion) and calculated the amount of dissolved fraction (see Appendices A). The proportion of extracted NPs from the total metal varied considerably across locations, ranging from 0.89 % to 11.60 % (mean 2.99 %) for Cu and 0.40 %–9.74 % (mean 3.59 %) for Pb. Positive correlations with mass concentrations suggest that NPs are more readily extracted at higher environmental levels. The dissolved fraction showed statistically significant negative correlations with NP characteristics, including mean size, particle mass, and number concentrations (Fig. A15, Table A13). This relationship reflects fundamental differences in metal partitioning. Samples with

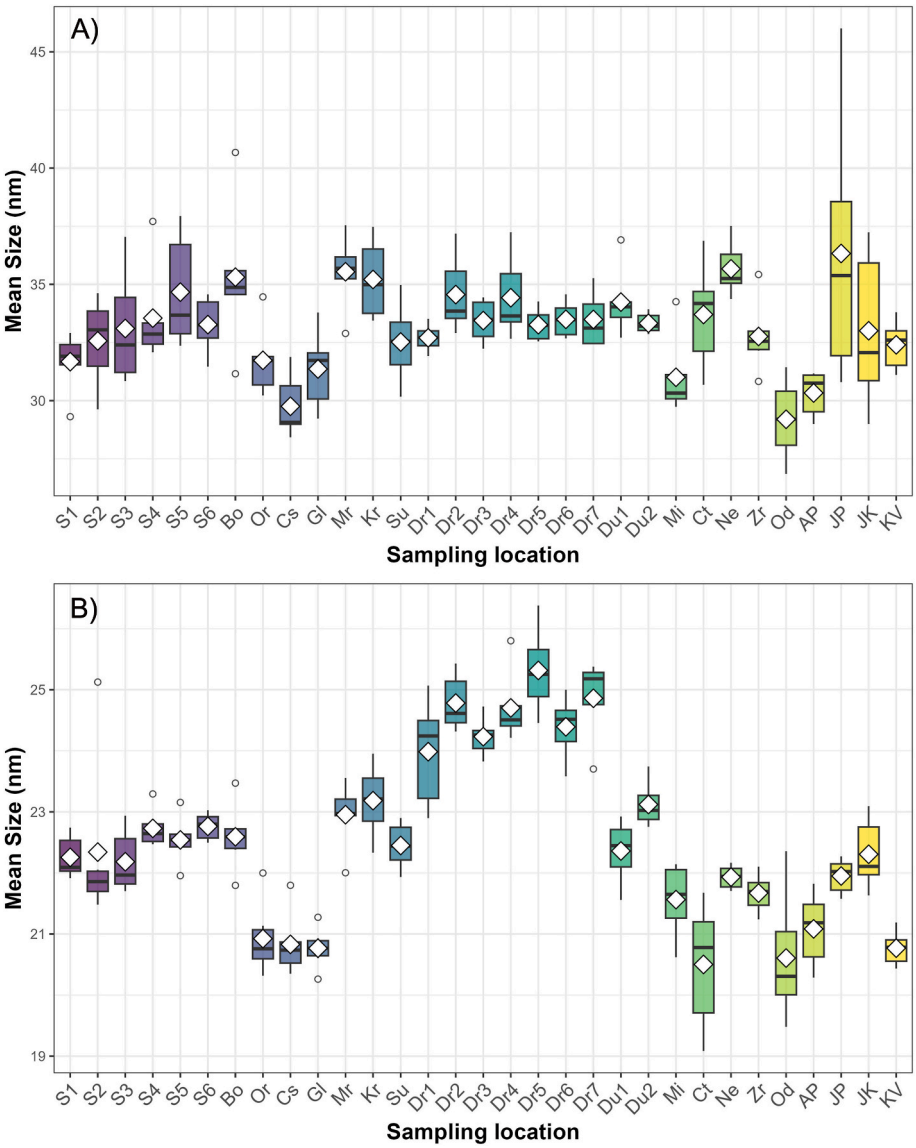

Fig. 6. Spatial trends of (A) Cu and (B) Pb NP size distribution across different catchment areas.

high dissolved fraction contain proportionally fewer detectable particles. Spatial patterns revealed distinct differences in metal forms depending on the source. Agricultural sites (Su, Cs, AP, Mi) exhibited high dissolved fractions (0.9–1), whereas urban-industrial sites demonstrated lower values (0.6–0.8). This pattern aligns with SEM-EDS characterization showing that agricultural sites contain more reactive Cu forms (CuO, $Cu(OH)_2$, $CuSO_4$ from fungicides) while urban-industrial sites contain more stable forms such as sulfides (Lučić et al., 2025). These differences have direct toxicological implications. Cu toxicity involves time-dependent dual pathways; the dissolved Cu^{2+} ions dominate short-term exposures, while nanoparticulate Cu drives chronic effects through oxidative stress and membrane damage (Ma et al., 2017). At environmentally relevant concentrations, CuO NPs dissolve within days to weeks (Gao et al., 2017), so both forms coexist in sediments. Agricultural sites with high dissolved fractions (0.9–1) therefore present dual exposure, containing readily bioavailable ionic Cu that causes acute toxicity and reactive Cu NPs that cause chronic particle-mediated effects. Two of these sites (Su, Mi) exceed the 1.94 μg g^{-1} threshold, indicating elevated NP concentrations coupled with high bioavailability. This represents a concerning combination for aquatic organisms.

Pb NPs displayed different behavior with lower and more variable dissolved fraction (0.4–0.9) across river and lake sediments. The relationship between proportion of extracted NPs and dissolved fraction for Pb was more complex than for Cu, reflecting the diverse nature of Pb sources and their mineral forms in sediments. Mining-derived PbS particles from the Drava River showed lower to intermediate values of dissolved fraction (0.37–0.68) with correspondingly higher proportion of extracted NPs (4.11–8.94 %), indicating that even relatively stable sulfide phases can be effectively mobilized under specific geochemical conditions. In contrast, industrial Pb-Sb alloy particles at Kr exhibited more uniform values of dissolved fraction (0.56–0.63) with moderate proportion of extracted NPs (2.87–5.20 %). These results align with findings from Lučić et al. (2025) for sewage sludge samples (dissolved fraction values of 0.54–0.80), which receive inputs from different urban sources including atmospheric deposition, stormwater runoff, and industrial discharges. The elevated Pb NP concentrations at sites Dr and Kr (7.55–25.4 μg g^{-1}), exceeding the 6.46 μg g^{-1} background threshold, correspond with total Pb levels (197–359 μg g^{-1}) known to cause ecological effects on benthic organisms (Besser et al., 2015). Furthermore, high nanoparticulate PbS concentrations present significant long-term ecological risks. PbS exhibits the fastest metal release rate among common metal sulfides (i.e., CuS or ZnS) under increasing dissolved oxygen and decreasing pH conditions (Chou et al., 2018). These factors can be triggered by flooding events and climate-driven soil

acidification in future scenarios (Jones et al., 2019).

Our findings offer practical support for implementing EU environmental directives concerning emerging contaminants. While NPs are not yet explicitly regulated under the Water Framework Directive (WFD) 2000/60/EC, the European Chemicals Agency (ECHA) revised the REACH Annexes in January 2020 to include nanomaterials. However, guidance for sediment assessment remains limited (Thit et al., 2024). Our validated methodology and threshold values may help address this gap by providing essential tools for nanomaterial risk assessment in sediment matrices. This work is a critical step toward establishing monitoring frameworks and environmental quality criteria for NPs as regulatory attention increasingly focuses on these emerging contaminants.

4. Conclusions and environmental implications

This study provides systematic baseline data on the occurrence, concentration, and trends of Cu and Pb NPs in freshwater sediments, addressing a critical knowledge gap in environmental NP research. We developed and validated a robust extraction and characterization method that reliably recovers metal-based NPs from complex sediment matrices. This method offers a practical tool for future monitoring, especially since NPs remain outside the specific regulatory scope of the Water Framework Directive (2000/60/EC). Our results reveal strong spatial heterogeneity in NP concentrations driven by localized anthropogenic sources. The statistically derived thresholds of 1.94 μg g^{-1} for Cu NPs and 6.46 μg g^{-1} for Pb NPs can serve as screening values for identifying elevated contamination in similar environmental settings. The amount of dissolved fraction for Cu is higher at agricultural sites, indicating greater metal reactivity and potential bioavailability in these areas. Given the well-established high toxicity of Cu and Pb NPs to freshwater organisms, particularly the smaller and more reactive particles observed in this study, these findings are relevant for ecological risk assessment and environmental management. Although further validation is recommended in regions with different lithology, climate, or anthropogenic pressures, this work provides a solid foundation and practical tools to support future regulation, monitoring, and mitigation of metal-containing NPs in freshwater ecosystems.

CRediT authorship contribution statement

Mavro Lučić: Writing – original draft, Validation, Methodology, Investigation, Data curation. **Janja Vidmar:** Writing – review & editing, Methodology. **Radmila Milačič Ščančar:** Writing – review & editing. **Janez Ščančar:** Writing – review & editing, Funding acquisition. **Bor Arah:** Writing – review & editing, Formal analysis. **Nevenka Mikac:** Writing – review & editing, Investigation. **Maja Ivanić:** Writing – review & editing, Data curation. **Željka Fiket:** Writing – review & editing. **Neda Vdović:** Writing – review & editing, Investigation, Data curation.

Declaration of competing interest

The authors declare that they have no known competing financial interests or personal relationships that could have appeared to influence the work reported in this paper.

Acknowledgements

This work was supported by the Slovenian Research and Innovation Agency (ARIS) through Program P1-0143. Mavro Lučić acknowledges funding for his research fellowship at the Jožef Stefan Institute through the European Union NextGenerationEU program. Additional support was provided by “Croatian Waters', the legal entity for water management in Croatia, under the program “Monitoring of Priority Contaminants in Biota and Sediment in Surface Freshwaters of the Republic of Croatia in 2019, 2020, 2021". We thank Dr. Kristina Pikelj for providing the geological map. We are also grateful to the three anonymous reviewers for their constructive comments and valuable suggestions that helped improve the quality of this manuscript.

Appendix A. Supplementary data

Supplementary data to this article can be found online at https://doi.org/10.1016/j.envres.2026.123787.

Data availability

Data are provided in the supplementary file.

References

Amiri, P., Behin, J., 2025. Fate of nanoparticles in aqueous environments: stability, physicochemical interactions, and separation. Sci. Total Environ. 1007, 180882. https://doi.org/10.1016/j.scitotenv.2025.180882.

Azimzada, A., Jreije, I., Hadioui, M., Shaw, P., Farner, J.M., Wilkinson, K.J., 2021. Quantification and characterization of Ti-, Ce-, and Ag-Nanoparticles in global surface waters and precipitation. Environ. Sci. Technol. 55 (14), 9836–9844. https://doi.org/10.1021/acs.est.1c00488.

Bačić, N., Mikac, N., Lučić, M., Sondi, I., 2021. Occurrence and distribution of technology-critical elements in recent freshwater and marine pristine Lake sediments in Croatia: a case study. Arch. Environ. Contam. Toxicol. 81, 574–588. https://doi.org/10.1007/s00244-021-00863-x.

Bao, Z., Al, T., Couillard, M., Poirier, G., Bain, J., Shrimpton, H.K., Finfrock, Y.Z., Lanzirotti, A., Paktunc, D., Saurette, E., Hu, Y., Ptacek, C.J., Blowes, D.W., 2021. A cross scale investigation of galena oxidation and controls on mobilization of lead in mine waste rock. J. Hazard. Mater. 412, 125130. https://doi.org/10.1016/j.jhazmat.2021.125130.

Besser, J.M., Ingersoll, C.G., Brumbaugh, W.G., Kemble, N.E., May, T.W., Wang, N., et al., 2015. Toxicity of sediments from lead–zinc mining areas to Juvenile Freshwater Mussels (Lampsilis siliquoidea) compared to standard test organisms. Environ. Toxicol. Chem. 34 (3), 626–639. https://doi.org/10.1002/etc.2849.

Brown, V.A., 2021. An introduction to linear mixed-effects modeling in R. Adv. Meth. Pract. psych. 4 (1). https://doi.org/10.1177/251524592096035.

Bundschuh, M., Filser, J., Lüderwald, S., McKee, M.S., Metreveli, G., Schaumann, G.E., Schulz, R., Wagner, S., 2018. Nanoparticles in the environment: where do we come from, where do we go to? Environ. Sci. Eur. 30, 1–17. https://doi.org/10.1186/s12302-018-0132-6.

Bundschuh, M., Seitz, F., Rosenfeldt, R.R., Schulz, R., 2016. Effects of nanoparticles in fresh waters: risks, mechanisms and interactions. Freshw. Biol. 61, 2185–2196. https://doi.org/10.1111/fwb.12701.

Chen, J., Wang, Z., Kang, K., Jiang, T., Ma, S., 2025. Microstructure and corrosion resistance of cutting rope Pb-Sb alloy: influence of heat treatment. J. Mater. Eng. Perform. 34, 24113–24123. https://doi.org/10.1007/s11665-025-10994-0.

Chiang, C.-W., Ng, D.-Q., Lin, Y.-P., Chen, P.-J., 2016. Dissolved organic matter or salts change the bioavailability processes and toxicity of the nanoscale tetravalent lead corrosion product PbO_2 to medaka fish. Environ. Sci. Technol. 50 (20), 11292–11301. https://doi.org/10.1021/acs.est.6b02072.

Chou, P.-I., Ng, D.-Q., Li, I.-C., Lin, Y.-P., 2018. Effects of dissolved oxygen, pH, salinity and humic acid on the release of metal ions from PbS, CuS and ZnS during a simulated storm event. Sci. Total Environ. 624, 1401–1410. https://doi.org/10.1016/j.scitotenv.2017.12.221.

Conway, J.R., Adeleye, A.S., Gardea-Torresdey, J., Keller, A.A., 2015. Aggregation, dissolution, and transformation of copper nanoparticles in natural waters. Environ. Sci. Technol. 49 (5), 2749–2756. https://doi.org/10.1021/es504918q.

Fiket, Ž., Mikac, N., Kniewald, G., 2017. Mass fractions of forty-six major and trace elements, including rare earth elements, in sediment and soil reference materials used in environmental studies. Geostand. Geoanal. Res. 41, 123–135. https://doi.org/10.1111/ggr.12129.

Gao, X., Spielman-Sun, E., Rodrigues, S.M., Casman, E.A., Lowry, G.V., 2017. Time and nanoparticle concentration affect the extractability of Cu from CuO NP-Amended soil. Environ. Sci. Technol. 51 (4), 2226–2234. https://doi.org/10.1021/acs.est.6b04705.

Ghosh, S., Sadhu, A., Mandal, A.H., Biswas, J.K., Sarkar, D., Saha, S., 2025. Copper oxide nanoparticles as an emergent threat to aquatic invertebrates and photosynthetic organisms: a synthesis of the known and exploration of the unknown. Curr. Pollut. Rep. 11, 6. https://doi.org/10.1007/s40726-024-00334-6.

Gottschalk, F., Ort, C., Scholzb, R.W., Nowack, B., 2011. Engineered nanomaterials in rivers e Exposure scenarios for Switzerland at high spatial and temporal resolution. Environ. Pollut. 159 (12), 3439–3445. https://doi.org/10.1016/j.envpol.2011.08.023.

Gottschalk, F., Debray, B., Klaessig, F., Park, P., Lacome, J.-M., Vignes, A., Portillo, V.P., Vázquez-Campos, S., Hendren, C.O., Lofts, S., Harrison, S., Svendsen, C., Kaegi, R., 2023. Predicting accidental release of engineered nanomaterials to the environment. Nat. Nanotechnol. 18, 412–418. https://doi.org/10.1038/s41565-022-01290-2.

Halamić, J., Peh, Z., Miko, S., Galović, L., Šorša, A., 2012. Geochemical Atlas of Croatia: environmental implications and geodynamical thread. J. Geochem. Explor. 115, 36–46. https://doi.org/10.1016/j.gexplo.2012.02.006.

Imfeld, G., Meite, F., Wiegert, C., Guyot, B., Masbou, J., Payraudeau, S., 2020. Do rainfall characteristics affect the export of copper, zinc and synthetic pesticides in surface runoff from headwater catchments? Sci. Total Environ. 741, 140437. https://doi.org/10.1016/j.scitotenv.2020.140437.

Jones, J.I., Murphy, J.F., Collins, A.L., Spencer, K.L., Rainbow, P.S., Arnold, A., Pretty, J. L., Moorhouse, A.M.L., Aguilera, V., Edwards, P., Parsonage, F., Potter, H., Whitehouse, P., 2019. The impact of metal-rich sediments derived from mining on freshwater stream life. In: de Voogt, P. (Ed.), Rev. Environ. Contam. Toxicol., 248, pp. 111–189.

Keller, A.A., Adeleye, A.S., Conway, J.R., Garner, K.L., Zhao, L., Cherr, G.N., Hong, J., Gardea-Torresdey, J.L., Godwin, H.A., Hanna, S., et al., 2017. Comparative environmental fate and toxicity of copper nanomaterials. NanoImpact 7, 28–40. https://doi.org/10.1016/j.impact.2017.05.003.

Keller, A.A., Ehrens, A., Zheng, Y., Nowack, B., 2023. Developing trends in nanomaterials and their environmental implications. Nat. Nanotechnol. 18, 834–837. https://doi.org/10.1038/s41565-023-01409-z.

Lead, J.R., Batley, G.E., Alvarez, P.J.J., Croteau, M.N., Handy, R.D., McLaughlin, M.J., Judy, J.D., Schirmer, K., 2018. Nanomaterials in the environment: behavior, fate, bioavailability, and effects-An updated review. Environ. Toxicol. Chem. 37 (8), 2029–2063. https://doi.org/10.1002/etc.4147.

Li, G., Liu, X., Wang, H., Liang, S., Xia, B., Sun, K., Li, X., Dai, Y., Yue, T., Zhao, J., Wang, Z., Xing, B., 2023. Detection, distribution and environmental risk of metal-based nanoparticles in a coastal bay. Water Res. 242, 120242. https://doi.org/10.1016/j.watres.2023.120242.

Li, Z., Hadioui, M., Wilkinson, K.J., 2025. Single particle inductively coupled plasma mass spectrometry for the characterization of colloidal particles in soils, sediments and sludges: comparative study of sector field and time-of-flight instruments. J. Anal. At. Spectrom. 40, 2487–2497. https://doi.org/10.1039/D5JA00181A.

Lockwood, T.E., Gonzalez De Vega, R., Clases, D., 2021. An interactive Python-based data processing platform for single particle and single cell ICP-MS. J. Anal. At. Spectrom. 36, 2536–2544. https://doi.org/10.1039/D1JA00297J.

Lučić, M., Mikac, N., Vdović, N., Bačić, N., Nava, V., Vidmar, J., Milačič, R., 2022. Spatial and temporal variability and sources of dissolved trace elements in the Sava River (Slovenia, Croatia). Environ. Sci. Pollut. Res. 29, 31734–31748. https://doi.org/10.1007/s11356-021-17769-9.

Lučić, M., Milačič Ščančar, R., Ščančar, J., Fiket, F., Arah, B., Vidmar, J., 2025. Optimized extraction, quantification and characterization of seven environmentally relevant metallic nanoparticles in sewage sludge: occurrence, composition and environmental risk assessment. J. Hazard. Mater. 497, 139734. https://doi.org/10.1016/j.jhazmat.2025.139734.

Ma, T., Gong, S., Tian, B., 2017. Effects of sediment-associated CuO nanoparticles on Cu bioaccumulation and oxidative stress responses in freshwater snail Bellamya aeruginosa. Sci. Total Environ. 580, 797–804. https://doi.org/10.1016/j.scitotenv.2016.12.026.

MacDonald, D.D., Ingersoll, C.G., Berger, T.A., 2000. Development and evaluation of consensus-based sediment quality guidelines for freshwater ecosystems. Arch. Environ. Contam. Toxicol. 39, 20–31. https://doi.org/10.1007/s002440010075.

Matys Grygar, T., Elznicová, J., Tůmová, Š., Kylich, T., Skála, J., Hron, K., Álvarez-Vázquez, M.A., 2023. Moving from geochemical to contamination maps using incomplete chemical information from long-term high-density monitoring of Czech agricultural soils. Environ. Earth Sci. 82, 6. https://doi.org/10.1007/s12665-022-10692-3.

Navratilova, J., Praetorius, A., Gondikas, A., Fabienke, W., Von der Kammer, F., Hofmann, T., 2015. Detection of engineered copper nanoparticles in soil using single particle ICP-MS. Int. J. Environ. Res. Publ. Health 12 (12), 15756–15768. https://doi.org/10.3390/ijerph121215020.

Ng, D.Q., Chu, Y., Tan, S.W., Wang, S.L., Lin, Y.P., Chu, C.H., Soo, Y.-L., Song, Y.-F., Chen, P.-J., 2018. In vivo evidence of intestinal lead dissolution from lead dioxide (PbO_2) nanoparticles and resulting bioaccumulation and toxicity in medaka fish. Environ. Sci. Nano 6 (2), 580–591. https://doi.org/10.1039/C8EN00893K.

Niu, Y., Chen, F., Li, Y., Ren, B., 2021. Trends and sources of heavy metal pollution in global river and Lake sediments from 1970 to 2018. In: de Voogt, P. (Ed.), Rev. Environ. Contam. Toxicol., 257. Springer, Cham, pp. 1–35. https://doi.org/10.1007/398_2020_59.

Pace, H.E., Rogers, N.J., Jarolimek, C., Coleman, V.A., Higgins, C.P., Ranville, J.F., 2011. Determining transport efficiency for the purpose of counting and sizing nanoparticles via single particle inductively coupled plasma mass spectrometry. Anal. Chem. 83, 9361–9369. https://doi.org/10.1021/ac201952t.

R core team, 2023. R: a Language and Environment for Statistical Computing. R Foundation for statistical computing, Vienna, Austria. http://www.R-project.org.

Ross, B.N., Knightes, C.D., 2022. Simulation of the environmental fate and transformation of nano copper oxide in a freshwater environment. ACS ES&T Water 2 (9), 1532–1543. https://doi.org/10.1021/acsestwater.2c00157.

Schindler, M., Santosh, M., Dottod, G., Silvae, L.F.O., Hochella, Jr. M.F., 2022. A review on Pb-bearing nanoparticles, particulate matter and colloids released from mining and smelting activities. Gondwana Res. 110, 330–346. https://doi.org/10.1016/j.gr.2021.07.011.

Thit, A., Skjolding, L.M., Hansen, S.F., 2024. Ecotoxicity testing of nanomaterials in sediment – suggestions to improve science and regulation. Environ. Sci. Nano 4, 1477–1486. https://doi.org/10.1039/D3EN00459G.

Tou, F., Wu, J., Fu, J., Niu, Z., Liu, M., Yang, Y., 2021. Titanium and zinc-containing nanoparticles in estuarine sediments: occurrence and their environmental implications. Sci. Total Environ. 754, 142388. https://doi.org/10.1016/j.scitotenv.2020.142388.

Trostle, K.D., Runyon, J.R., Pohlmann, M.A., Redfield, S.E., Pelletier, J., McIntosh, J., Chorover, J., 2018. Colloids and organic matter complexation control trace metal concentration-discharge relationships in Marshall Gulch stream waters. Water Resour. Res. 52 (10), 7931–7944. https://doi.org/10.1002/2016WR019072.

Vidmar, J., Zuliani, T., Milačič, R., Ščančar, J., 2022. Following the occurrence and origin of titanium dioxide nanoparticles in the Sava river by single particle ICP-MS. Water 14 (6), 959. https://doi.org/10.3390/w14060959.

Vdović, N., Lučić, M., Mikac, N., Bačić, N., 2021. Partitioning of metal contaminants between bulk and fine-grained fraction in freshwater sediments: a critical appraisal. Minerals 11, 603. https://doi.org/10.3390/min11060603.

Wang, Z., Zhang, L., Zhao, J., Xing, B., 2016. Environmental processes and toxicity of metallic nanoparticles in aquatic systems as affected by natural organic matter. Environ. Sci. Nano 3, 240–255. https://doi.org/10.1039/C5EN00230C.

Worms, I.A.M., Tharaud, M., Gasco, R., Montaño, M.D., Goodman, A., Slaveykova, V.I., Benedetti, M.F., Churchill, C.M., Fernando, S., Alasonati, E., Moens, C., Cuss, C.W., 2025. Exploring environmental nanobiogeochemistry using field-flow fractionation and ICP-MS-based tools: progress and frontiers. Environ. Sci. Nano 12 (8), 3821–3846. https://doi.org/10.1039/D5EN00096C, 4.

Ying, S., Liu, Z., Hu, Y., Peng, R., Zhu, X., Dong, S., Yan, D., Huang, Y., 2024. Location-dependent occurrence and distribution of metal-based nanoparticles in bay environments. J. Hazard. Mater. 476, 134972. https://doi.org/10.1016/j.jhazmat.2024.134972.

Zhao, X., Niu, Z., Xu, M., Wu, L., Wang, M., Shi, Z., Cui, Y., Chen, J., Yang, Y., 2025. Source-specific fingerprints and machine learning-driven apportionment of lead-containing fine particles from typical industrial emissions in China. J. Hazard. Mater. 499, 140173. https://doi.org/10.1016/j.jhazmat.2025.140173.

Zheng, R., Li, L., Wu, Z., Xu, A., Xu, H., Hao, Z., Yu, S., Cai, Y., Liu, J., 2025. Distribution and source of titanium dioxide nanoparticles in seawater and sediment from Jiaozhou Bay, China. J. Hazard. Mater. 483, 136576. https://doi.org/10.1016/j.jhazmat.2024.13657.

Žerdoner, T., Vidmar, J., Arah, B., Zuliani, T., 2025. Determination of airborne metal-containing nanoparticles in a historic mining area using single particle ICP-MS. Analyst 150, 4572–4585. https://doi.org/10.1039/D5AN00480B.